MINIMUM TRIM DRAG DESIGN FOR INTERFERING LIFTING SURFACES USING VORTEX-LATTICE METHODOLOGY

John E. Lamar
NASA Langley Research Center

SUMMARY

A new subsonic method has been developed by which the mean camber surface can be determined for trimmed noncoplanar planforms with minimum vortex drag. This method uses a vortex lattice and overcomes previous difficulties with chord loading specification. This method uses a Trefftz plane analysis to determine the optimum span loading for minimum drag, then solves for the mean camber surface of the wing, which will provide the required loading. Pitching-moment or root-bending-moment constraints can be employed as well at the design lift coefficient.

Sensitivity studies of vortex-lattice arrangement have been made with this method and are presented. Comparisons with other theories show generally good agreement. The versatility of the method is demonstrated by applying it to (1) isolated wings, (2) wing-canard configurations, (3) a tandem wing, and (4) a wing-winglet configuration.

INTRODUCTION

Configuration design for subsonic transports usually begins with the wing, after which the body and its effects are taken into account, and then the tails are sized and located by taking into account stability and control requirements. With the advent of highly maneuverable aircraft having closely coupled lifting surfaces, there has been an increased interest in changing the design order so that multiple surfaces could be designed together to yield a trimmed configuration with minimum induced drag at some specified lift coefficient. Such a combined design approach requires that the mutual interference of the lifting surfaces be considered initially.

Single planform design methods are available to optimize the mean camber surface, better called the local elevation surface, for wings flying at subsonic speeds (for example, ref. 1) and at supersonic speeds (for example, refs. 2 and 3). The design method presented in reference 1 was developed from an established analysis method (Multhopp type), also presented in reference 1, by using the same mathematical model, but the design method solves for the local mean slopes rather than the lifting pressures. In the usual implementation of reference 1, the design lifting pressures are taken to be linear chordwise, but must be represented in this solution by a sine series which oscillates about them. An example presented herein demonstrates that corresponding oscillations may appear in pressure distributions measured on wings which have been designed by the method of reference 1. The method developed herein overcomes this oscillatory lifting pressure behavior by specifying linear chord loadings at the outset.

The development approach used in the two-planform design problem will be similar to that used for a single planform. The analytic method employed, selected because of its geometric versatility, is the noncoplanar two-planform vortex-lattice method of reference 4.

The design procedure is essentially an optimization or extremization problem. Subsonic methods (for example, see refs. 5 and 6) are available for determining the span load distributions on bent lifting lines in the Trefftz plane, but they do not describe the necessary local elevation surface. This is one of the objectives of the present method which will utilize the Lagrange multiplier technique (also employed in refs. 2 and 3). The method of reference 4 is used to provide the needed geometrical relationships between the circulation and induced normal flow for complex planforms, as well as to compute the lift, drag, and pitching moment.

This paper presents limited results of precision studies and comparisons with other methods and data and is a condensed version of reference 7. Several examples of solutions for configurations of recent interest are also presented.

SYMBOLS

$A_{l,n}$ element of aerodynamic influence function matrix A which contains induced normal flow at lth point due to nth horseshoe vortex of unit strength; total number of elements is $\frac{N}{2} \times \frac{N}{2}$

AR aspect ratio

a fractional chord location where chord load changes from constant value to linearly varying value toward zero at trailing edge

a_i, b_i, c_i coefficients in spanwise scaling polynomial

b wing span

C_D drag coefficient

$C_{D,o}$ drag coefficient at $C_L = 0$

$C_{D,v}$ vortex or induced drag coefficient, $\frac{\text{Vortex drag}}{q_\infty S_{ref}}$

C_L lift coefficient, $\frac{\text{Lift}}{q_\infty S_{ref}}$

C_m pitching-moment coefficient about $\bar{Y}$-axis, $\frac{\text{Pitching moment}}{q_\infty S_{ref} c_{ref}}$

ΔC_p lifting pressure coefficient

c chord

c_l	section lift coefficient
c_{ref}	reference chord
I	$\equiv \left[\bar{N}_c a + 0.75\right]$ (brackets indicate "take the greatest integer")
K	maximum number of spanwise scaling terms in solution technique for wings without dihedral
L	lift
$M_{\bar{Y}}$	pitching moment about coordinate origin
M_∞	free-stream Mach number
m	number of span stations where pressure modes are defined as used in reference 1
N	maximum number of elemental panels on both sides of configuration; maximum number of chordal control points at each of m span stations as used in reference 1
$\bar{N}_c$	number of elemental panels from leading to trailing edge in chordwise row
$\bar{N}_s$	total number of (chordwise) rows in spanwise direction of elemental panels on configuration semispan
q_∞	free-stream dynamic pressure
S_{ref}	reference area
s	horseshoe vortex semiwidth in plane of horseshoe (see fig. 1)
U	free-stream velocity
X,Y,Z	axis system of given horseshoe vortex (see fig. 1)
$\bar{X},\bar{Y},\bar{Z}$	body-axis system for planform (see fig. 1)
$\hat{X},\hat{Y},\hat{Z}$	wind-axis system for planform (see sketch (a))
x,y,z	distance along X-, Y-, and Z-axis, respectively
$\bar{x},\bar{y},\bar{z}$	distance along $\bar{X}$-, $\bar{Y}$-, and $\bar{Z}$-axis, respectively
$\Delta\bar{x}$	incremental movement of $\bar{X}$-$\bar{Y}$ coordinate origin in streamwise direction

y^*, z^*	y and z distances from image vortices located on right half of plane of symmetry, as viewed from behind, to points on left panel
$\bar{z}_c$	canard height with respect to wing plane, positive down
$\bar{z}/c$	local elevation normalized by local chord, referenced to local trailing-edge height, positive down
$(\partial\bar{z}/\partial\bar{x})_l$	lth elemental local slope in vector $\{\partial\bar{z}/\partial\bar{x}\}$ of N/2 elements (see eq. (1))
α	angle of attack, deg
Γ_n	vortex strength of nth element in vector $\{\Gamma\}$ of N/2 elements
ϵ	incidence angle, positive leading edge up, deg
δ	independent variable in extremization process
η_l	nondimensional spanwise coordinate based on local planform semispan
ξ	distance along local chord normalized by local chord
ξ'	fractional chordwise location of point where mean camber height is to be computed (see eq. (14))
σ,σ'	dihedral angle from trailing vortex to point on left panel being influenced; σ measured from left panel, σ' measured from right panel
ϕ	horseshoe vortex dihedral angle in $\bar{Y}$-$\bar{Z}$ plane on left wing panel, deg
ϕ'	horseshoe vortex dihedral angle on right wing panel, $\phi' = -\phi$, deg

Subscripts:

c	canard
d	design
i,j,k	indices to vary over the range indicated
le	leading edge
l,n	associated with slope point and horseshoe vortex, respectively, ranging from 1 to N/2
L	left trailing leg

R right trailing leg

ref reference value

w wing

Matrix notation:

{ } column vector

[ ] square matrix

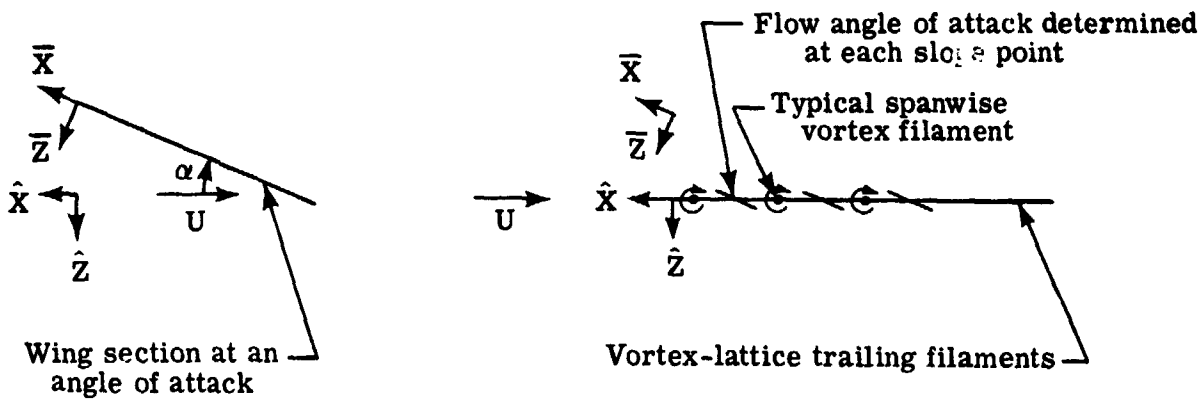

Sketch (a)

THEORETICAL DEVELOPMENT

This section presents the application of vortex-lattice methodology to the mean-camber-surface design of two lifting planforms which may be separated vertically and have dihedral. For a given planform, local vertical displacements of the surfaces with respect to their chord lines in the wing axis (see sketch (a)) are assumed to be negligible; however, vertical displacements of the solution surfaces due to planform separation or dihedral are included. The wakes of these bent lifting planforms are assumed to lie in their respective extended bent chord planes with no roll up. For a two-planform configuration the resulting local elevation surface solutions are those for which both the vortex drag is minimized at the design lift coefficient and the pitching moment is constrained to be zero about the origin. For an isolated planform no pitching-moment constraint is imposed. Thus, the solution is the local elevation surface yielding the minimum vortex drag at the design lift coefficient. Lagrange multipliers together with suitable interpolating and integrating procedures are used to obtain the solutions. The details of the solution are given in the following five subsections.

Relationship Between Local Slope and Circulation

From reference 4, the distributed circulation over a lifting system is related to the local slope by

$$\left\{\frac{\partial \bar{z}}{\partial \bar{x}}\right\} = [A]\left\{\frac{\Gamma}{U}\right\} \tag{1}$$

where the matrix [A] is the aerodynamic influence coefficient matrix based on the paneling technique described in reference 4.

Circulation Specification

Once the surface slope matrix $\{\partial \bar{z}/\partial \bar{x}\}$ is known, chordwise integration can be performed to determine the local elevation surface $\bar{z}/c$, which contains the effects of camber, twist, and angle of attack. The major problem to be solved is determining the necessary circulation matrix $\{\Gamma/U\}$ to employ in equation (1). The problem is simplified somewhat by having the chordwise shape of the bound circulation remain unchanged across each span, although the chordwise shape may vary from one planform to another. The chordwise loadings allowable in the program range from rectangular to right triangular toward the leading edge and were selected because they are of known utility. An example is given in figure 2. Two different techniques are utilized to arrive at the spanwise scaling of the chordwise shapes. The particular technique to be employed depends on whether the configuration has dihedral.

For a configuration having dihedral, the spanwise scaling must be determined discretely because no finite polynomial representation of the scaling is known with certainty, even for ar isolated wing. However, for configurations with no dihedral, the spanwise scaling can be written as a polynomial for each planform,

$$\sqrt{1 - \eta_l^2}\left(a_i + b_i\eta_l^2 + c_i\eta_l^4\right)$$

(see fig. 2) with a maximum of three coefficients per planform being determined as part of the solution. It is possible to write this polynomial as a solution because the isolated wing solution is known to be of the elliptical form $\sqrt{1 - \eta_l^2}$, and the presence of the other planform is assumed to generate a loading disturbance which can be represented by the other two terms in addition to adjusting a_i. Once the scaling is known from either technique, then $\{\Gamma/U\}$ is readily obtained by multiplication.

Lift, Pitching-Moment, and Drag Contributions

The contributions to C_L and to C_m, respectively, from the jth chordwise row of horseshoe vortices are

$$C_{L,j} = \frac{L_j}{q_\infty S_{ref}} = \frac{4q_\infty s \cos \phi_j}{q_\infty S_{ref}} \sum_{i=1}^{\bar{N}_c} \left(\frac{\Gamma}{U}\right)_i \tag{2}$$

and

$$C_{m,j} = \frac{M_{\bar{Y},j}}{q_\infty S_{ref} c_{ref}} = \frac{4 q_\infty s \cos \phi_j}{q_\infty S_{ref} c_{ref}} \sum_{i=1}^{\bar{N}_c} \left(\frac{\Gamma}{U}\right)_i \bar{x}_{j,i} \tag{3}$$

where

$$\left(\frac{\Gamma}{U}\right)_i \equiv \begin{cases} 1 & \left(\xi_i \leq a\right) \\ \dfrac{1 - \xi_i}{1 - a} & \left(\xi_i > a\right) \end{cases} \tag{4a}$$

$$\xi_i \equiv \frac{i - 0.75}{\bar{N}_c} \tag{4b}$$

and

$$\bar{x}_{j,i} \equiv \left(\bar{x}_{le}\right)_j - \left(\frac{i - 0.75}{\bar{N}_c}\right) c_j \tag{5}$$

Even though $C_{L,j}$ and $C_{m,j}$ actually occur on the wing at the jth spanwise location, they can be utilized in a Trefftz plane solution if the chordwise summations are performed. This utilization is possible herein because the trailing wake is assumed not to roll up, and the general configuration has specifiable chord loading shapes. Summing the chordwise loadings at this point allows the solution of the spanwise scaling to be performed on a bent lifting line located in the Trefftz plane, which is, of course, ideally suited for the vortex drag computation. In addition, the summation reduces the number of unknowns from the product of $\bar{N}_c$ and $\bar{N}_s$ to only $\bar{N}_s$. Hence, a larger value of $\bar{N}_s$ can be used in the Trefftz plane, which should yield improved accuracy in the spanwise scaling factors without affecting the number of horseshoe vortices on the wing. Then, when the circulations are needed on the wing for use in equation (1), the well-defined variations of the spanwise scaling factors are interpolated to the original spanwise positions of the wing vortex lattice which is used to generate [A]. The procedure is implemented as follows:

The summation in the lift expression (eq. (2)) can be written as

$$\sum_{i=1}^{\bar{N}_c} \left(\frac{\Gamma}{U}\right)_i = \sum_{i=1}^{I} \left(\frac{\Gamma}{U}\right)_i + \sum_{i=I+1}^{\bar{N}_c} \left(\frac{\Gamma}{U}\right)_i \tag{6}$$

where I is the last i value which satisfies $\xi_i \leq a$; that is,

$$I \equiv \left[\bar{N}_c a + 0.75\right] \tag{7}$$

where the brackets indicate "take the greatest integer." Hence,

$$\sum_{i=1}^{\bar{N}_c} \left(\frac{\Gamma}{U}\right)_i = I + \frac{\left(\bar{N}_c + 0.75\right)\left(\bar{N}_c - I\right)}{\bar{N}_c(1 - a)} - \frac{1}{\bar{N}_c(1 - a)} \sum_{i=I+1}^{\bar{N}_c} i \tag{8}$$

Similarly, the summation in the pitch expression (eq. (3)) can be written as

$$\sum_{i=1}^{\bar{N}_c} \left(\frac{\Gamma}{U}\right)_i \bar{x}_{j,i} = \left[\left(\bar{x}_{le}\right)_j + \frac{0.75c_j}{\bar{N}_c}\right]\left[I + \frac{\left(\bar{N}_c + 0.75\right)\left(\bar{N}_c - I\right)}{\bar{N}_c(1 - a)}\right] - \frac{c_j}{\bar{N}_c} \sum_{i=1}^{I} i$$

$$- \frac{1}{\bar{N}_c(1 - a)}\left[\left(\bar{x}_{le}\right)_j + c_j + \frac{1.5c_j}{\bar{N}_c}\right] \sum_{i=I+1}^{\bar{N}_c} i$$

$$+ \frac{c_j}{\bar{N}_c^{\,2}(1 - a)} \sum_{i=I+1}^{\bar{N}_c} i^2 \tag{9}$$

The contribution to the vortex drag coefficient at the ith chordwise row due to the jth chordwise row is obtained by using only half the trailing vortex induced normal wash from the Trefftz plane. The result is

$$C_{D,i,j} = \frac{s}{\pi S_{ref}} \left[\sum_{i=1}^{\bar{N}_c} \left(\frac{\Gamma}{U}\right)_i \sum_{j=1}^{\bar{N}_c} \left(\frac{\Gamma}{U}\right)_j \right] \left[\frac{\pm\cos\left(\sigma_{L,i,j} - \phi_i\right)}{\sqrt{\left(y_{i,j} + s\cos\phi_j\right)^2 + \left(z_{i,j} + s\sin\phi_j\right)^2}} \right.$$

$$- \frac{\pm\cos\left(\sigma_{R,i,j} - \phi_i\right)}{\sqrt{\left(y_{i,j} - s\cos\phi_j\right)^2 + \left(z_{i,j} - s\sin\phi_j\right)^2}}$$

$$- \frac{\cos\left(\sigma'_{L,i,j} - \phi_i\right)}{\sqrt{\left(y^*_{i,j} + s\cos\phi'_j\right)^2 + \left(z^*_{i,j} + s\sin\phi'_j\right)^2}}$$

$$\left. + \frac{\cos\left(\sigma'_{R,i,j} - \phi_i\right)}{\sqrt{\left(y^*_{i,j} - s\cos\phi'_j\right)^2 + \left(z^*_{i,j} - s\sin\phi'_j\right)^2}} \right] \tag{10}$$

In the ± sign, plus indicates that the trailing vortex filament is to the left of the influenced point; minus, to the right.

In using equations (2), (3), and (10), a new vortex system is set up in the Trefftz plane in which the bent chord plane is represented by a system of uniformly spaced trailing vortices (the quantity $2s$ in fig. 1). This uniformity of vortex spacing leads to a simplification in the equations and can be thought of as a discretization of the ideas of Munk (ref. 8) and Milne-Thomson (ref. 9) for a bound vortex of constant strength.

Spanwise Scaling Determination

To determine the spanwise scaling with either technique requires the combination of the contributions from each spanwise position for configurations with dihedral or the mode shape contributions for configurations without dihedral. These contributions must be employed in the appropriate total C_L and C_m constraint equations as well as in the $C_{D,v}$ extremization operation. Due to limited space only the solution for wings without dihedral will be discussed. The equations to be employed in the Lagrange extremization method are

$$C_L = 2 \sum_{k=1}^{K} \delta_k C_{L,k} \tag{11}$$

$$C_m = 2 \sum_{k=1}^{K} \delta_k C_{m,k} \tag{12}$$

and

$$C_{D,v} = 2 \sum_{i=1}^{K} \sum_{k=1}^{K} \delta_i C_{D,i,k} \delta_k \tag{13}$$

where $K \leq 6$ and $C_{L,k}$ and $C_{m,k}$ are the C_L and C_m contributions associated with the kth term in the polynomials

$$\sqrt{1 - \eta_1^2}\left(\delta_1 + \delta_2 \eta_1^2 + \delta_3 \eta_1^4\right)$$

or

$$\sqrt{1 - \eta_1^2}\left(\delta_4 + \delta_5 \eta_1^2 + \delta_6 \eta_1^4\right)$$

(Note that $k = 1$, 2, and 3 are assigned to the first planform and 4, 5, and 6 to the second.) These contributions are computed by first assuming a unit value of scaling with each term in the polynomial, then multiplying each resulting spanwise scaling distribution by the $C_{L,j}$ and $C_{m,j}$ terms of equations (2) and (3), and finally summing spanwise over all the chordwise rows associated with each set of k values (or planform). The vortex drag coefficient associated with the ith and kth combination of spanwise scaling distributions $C_{D,i,k}$ is compared similarly. The δ_k terms are equivalent to the unknown coefficients in the polynomial and are the independent variables in the solution.

An application of the preceding process to a conventional wing-tail configuration is shown in figure 3. The resulting idealized loading set is of the type that would meet the constraints and extremization.

Determination of Local Elevation Curves

With δ_k known, then $\{\Gamma/U\}$, C_L, C_m, and $C_{D,v}$ can be determined. The results for $\{\Gamma/U\}$ are interpolated to the original spanwise positions of the paneling which is used in equation (1) and in the following equation to find the local elevation curves. The equation for the local elevation above the computational plane at a particular point $(\xi', \bar{y})$ is

$$\frac{\bar{z}}{c}(\xi', \bar{y}) = \int_1^{\xi'} \frac{\partial \bar{z}}{\partial \bar{x}}(\xi, \bar{y})\, d\xi \tag{14}$$

RESULTS AND DISCUSSION

General

It is necessary to examine the sensitivity of the results of the present method to vortex-lattice arrangement. It is also important to compare results obtained with this method with those available in the literature. Unfortunately, the available solutions, whether exact or numerical, may not be for configurations which will exercise the constraint or extreminization capabilities of the present method. In fact, the available exact solutions are for configurations which are either two-dimensional sections or isolated three-dimensional wings with a nonelliptic span loading. The solutions for such configurations require program modifications to the span loading and involve no optimization.

Two-Dimensional Comparison

Various chordwise arrangements and number of vortices were investigated for several chordwise loading shapes, of which the $a = 0.6$ results are given in figure 4. Although difficult to see clearly from this figure, the agreement of the present method with analytic results (ref. 10) is good for both local slope and elevation. Examination of figure 4 leads to the following general conclusions concerning the chordwise arrangement: (1) Uniform spacing is preferred; (2) $\bar{N}_c = 20$ is a good compromise when considering both computational requirements and completely converged results. An additional conclusion is that the present method yields incidence angles near the leading edge which are slightly higher than the analytical ones.

Number of Rows Along Semispan $\left(\bar{N}_s\right)$

Various spanwise arrangements and number of vortices were studied for one planform and from these studies the following conclusions were drawn: (1) Uniform spacing is preferred; (2) for at least 10 spanwise rows per semispan, the local slopes and elevations were not too sensitive to increasing the number.

Three-Dimensional Comparisons

Two comparisons with available mean-camber-surface solutions will be made. The comparisons are for a high-aspect-ratio sweptback and tapered wing with a uniform area loading at $C_{L,d} = 1.0$ and $M_\infty = 0.96$ and a lower aspect-ratio trapezoidal wing with $a = 1.0$, spanwise elliptic loading at $C_{L,d} = 0.35$, and $M_\infty = 0.40$.

Figure 5 presents the predicted results from the present method for the sweptback wing and compares these results with those from references 1 and 11. A comparison of the three solutions indicates that they are all in generally good agreement with the exception of the results at $\frac{\bar{y}}{b/2} = 0.05$. The surprising result is that the present method and the modified Multhopp method (ref. 1) agree as well as they do at this span station because of the known differences that exist between them near the plane of symmetry. The reason for the larger disagreement between the present method and that of reference 11 near $\frac{\bar{y}}{b/2} = 0$

is not clear, but this disagreement may be caused by the different $\bar{N}_c$ values utilized by the two methods. Reference 11 effectively uses an infinite number since over each infinitesimal span strip across the wing the method locates a single quadrilateral vortex around the periphery of the enclosed area. This vortex extends from the leading edge to the trailing edge and includes segments of the edges as well. For a uniform area loading, the trailing leg parts of the quadrilateral vortices cancel with adjacent spanwise ones all across the wing. This leaves only the edge segments to contribute to the induced flow field. The present method utilizes a numerical rather than a graphical solution in order to provide a general capability; hence, $\bar{N}_c$ values are limited as discussed previously. Also, vortices are not placed around the leading and trailing edges in the present method.

A comparison of the present design method with that of reference 1 is shown in figure 6 for a lower aspect-ratio trapezoidal wing. The local slopes and elevations determined by the two methods are in reasonably close agreement at the three spanwise locations detailed; however, an oscillatory trend is evident in the local slopes obtained from the method of reference 1 (fig. 6(a)). These oscillations apparently originate in the truncated sine series used in reference 1 to represent a uniform chordwise distribution. Integration of the local slopes to obtain local elevations tends to suppress the oscillations (fig. 6(b)); however, the local pressures depend upon the slope rather than the elevation. Consequently, the measured chordwise pressure distribution will demonstrate the same oscillatory character. A model built according to the design of reference 1 was tested (ref. 12), and the measured pressure distributions for a typical spanwise location (fig. 6(c)) indicate that indeed the oscillations are present. Presumably, similar measurements on a model designed by the present method would not behave in this manner since the input loadings are truly linear.

Force tests (ref. 13) of an essentially identical model indicate that the measured drag polar was tangent to $C_D = C_{D,o} + \frac{C_L^2}{\pi AR}$; that is, the vortex drag was indeed a minimum at the design C_L (or 100 percent leading-edge suction was obtained). It is presumed from the small differences in local slope between the present method and the method of reference 1 that a similar result would be obtained for a design by the present method.

Application to a Wing-Canard Combination

The present method has been demonstrated by optimizing a wing-canard combination (fig. 7). To illustrate how the span load optimizing feature operates with the constraints, figure 8 presents individual and total span load distributions for various values of a_c and a_w with the moment trim point at $\frac{\Delta\bar{x}}{b/2} = 0.1$ and $\frac{\bar{z}_c}{b/2} = 0$. (This trim point is given with respect to the axis system shown in the sketch in figure 9.) From figure 8 there are three important observations to be made: (1) The individual span loadings change in the anticipated direction with the changing chord loadings in order to meet the same C_L and C_m constraints; (2) the total span loading does not change; (3) consequently, the vortex drag of the configuration is constant, as would be anticipated from Munk's stagger theorem.

The effects of varying the vertical separation and the moment trim point on the resulting drag and span loadings are also illustrated (figs. 9 and 10). All surfaces are designed for $C_{L,d} = 0.2$, $a_c = 0.6$, $a_w = 0.8$, and $M_\infty = 0.30$ and have $C_m = 0$ about the moment trim point. Figure 9 shows that for all vertical separations, moving the moment trim point forward increases the vortex drag over some range, and furthermore, increasing the out-of-plane vertical separation reduces the vortex drag. Of course, not all moment trim points utilized will produce a stable configuration. These variations illustrate the importance of balancing the lift between the two lifting surfaces so that for some reasonable moment trim point and vertical separation, the vortex drag will be at a minimum. The minimum point on each vortex drag curve occurs with the pitching-moment constraint not affecting the extremization.

Figure 10 presents the individual span loadings with increasing vertical separation $\left(\frac{\bar{z}_c}{b/2} < 0 \text{ above the wing plane}\right)$ with $a_c = 0.6$ and $a_w = 0.8$. There are three observations which can be made from these results for increasing vertical separation: (1) The individual span loadings tend to become more elliptical; (2) consequently, the vortex drag decreases; (3) the individual lift contributions show only a little sensitivity to separation distance once the canard is above the wing when compared with the coplanar results.

Application to Tandem Wing Design

This design method has been employed in the determination of the local elevation surfaces for a tandem wing. Figure 11 shows a sketch of a tandem wing configuration and selected results taken from the wind-tunnel tests made with a model based on this design at a Mach number of 0.30 (ref. 14). At $C_{L,d} = 0.35$ the vortex drag increment is correctly estimated. The measured C_m is slightly positive (0.02). Reference 14 states that a part of the C_m error (C_m should be zero) is a result of a difference in the fuselage length between the designed and constructed model.

Design of a Wing-Winglet Configuration

Figure 12 presents the wing-winglet combination of interest along with pertinent aerodynamic characteristics and local elevations obtained from the present method. For comparison these same items are calculated with a program modification that adds a root-bending-moment constraint to produce the same moment that would be obtained on the original wing extending to the plane of symmetry but without its basic wingtip. The assumed span loading is elliptical. The force and moment coefficients are based on the wing outside of a representative fuselage and without the basic wingtip.

The results of this comparison are as follows: (1) The root-bending-moment constraint increases the vortex drag slightly because of the changes in the $c_l c$ distribution required; (2) the differences in local elevations are confined primarily to the outer 50 percent semispan and result mainly from the differences in the incidence angles; (3) significant amounts of incidence are required in the winglet region with or without the root-bending-moment constraint.

CONCLUDING REMARKS

A new subsonic method has been developed by which the mean camber (local elevation) surface can be determined for trimmed noncoplanar planforms with minimum vortex drag. This method employs a vortex lattice and overcomes previous difficulties with chord loading specification. This method designs configurations to have their local midsurface elevations determined to yield the span load for minimum vortex drag while simultaneously controlling the pitching-moment or root-bending-moment constraint at the design lift coefficient. This method can be used for planforms which (1) are isolated, (2) are in pairs, (3) include a winglet, or (4) employ variable sweep, but only at a specified sweep position.

Results obtained with this method are comparable with those from other methods for appropriate planforms. The versatility of the present method has been demonstrated by application to (1) isolated wings, (2) wing-canard configurations, (3) a tandem wing, and (4) a wing-winglet configuration.

REFERENCES

1. Lamar, John E.: A Modified Multhopp Approach for Predicting Lifting Pressures and Camber Shape for Composite Planforms in Subsonic Flow. NASA TN D-4427, 1968.

2. Carlson, Harry W.; and Middleton, Wilbur D.: A Numerical Method for the Design of Camber Surfaces of Supersonic Wings With Arbitrary Planforms. NASA TN D-2341, 1964.

3. Sorrells, Russell B.; and Miller, David S.: Numerical Method for Design of Minimum-Drag Supersonic Wing Camber With Constraints on Pitching Moment and Surface Deformation. NASA TN D-7097, 1972.

4. Margason, Richard J.; and Lamar, John E.: Vortex-Lattice FORTRAN Program for Estimating Subsonic Aerodynamic Characteristics of Complex Planforms. NASA TN D-6142, 1971.

5. Lundry, J. L.: A Numerical Solution for the Minimum Induced Drag, and the Corresponding Loading, of Nonplanar Wings. NASA CR-1218, 1968.

6. Loth, John L.; and Boyle, Robert E.: Optimum Loading on Nonplanar Wings at Minimum Induced Drag. Aerosp. Eng. TR-19 (Contract N00014-68-A-1512), West Virginia Univ., Aug. 1969. (Available from DDC as AD 704 502.)

7. Lamar, John E.: A Vortex-Lattice Method for the Mean Camber Shapes of Trimmed Noncoplanar Planforms With Minimum Vortex Drag. NASA TN D-8090, 1976.

8. Munk, Max M.: The Minimum Induced Drag of Aerofoils. NACA Rep. 121, 1921.

9. Milne-Thomson, L. M.: Theoretical Aerodynamics. Second ed. D. Van Nostrand Co., Inc., 1952.

10. Abbott, Ira H.; Von Doenhoff, Albert E.; and Stivers, Louis S., Jr.: Summary of Airfoil Data. NACA Rep. 824, 1945. (Supersedes NACA WR L-560.)

11. Katzoff, S.; Faison, M. Frances; and DuBose, Hugh C.: Determination of Mean Camber Surfaces for Wings Having Uniform Chordwise Loading and Arbitrary Spanwise Loading in Subsonic Flow. NACA Rep. 1176, 1954. (Supersedes NACA TN 2908.)

12. Henderson, William P.: Pressure Distributions on a Cambered Wing-Body Configuration at Subsonic Mach Numbers. NASA TN D-7946, 1975.

13. Henderson, William P.; and Huffman, Jarrett K.: Effect of Wing Design on the Longitudinal Aerodynamic Characteristics of a Wing-Body Model at Subsonic Speeds. NASA TN D-7099, 1972.

14. Henderson, William P.; and Huffman, Jarrett K.: Aerodynamic Characteristics of a Tandem Wing Configuration at a Mach Number of 0.30. NASA TM X-72779, 1975.

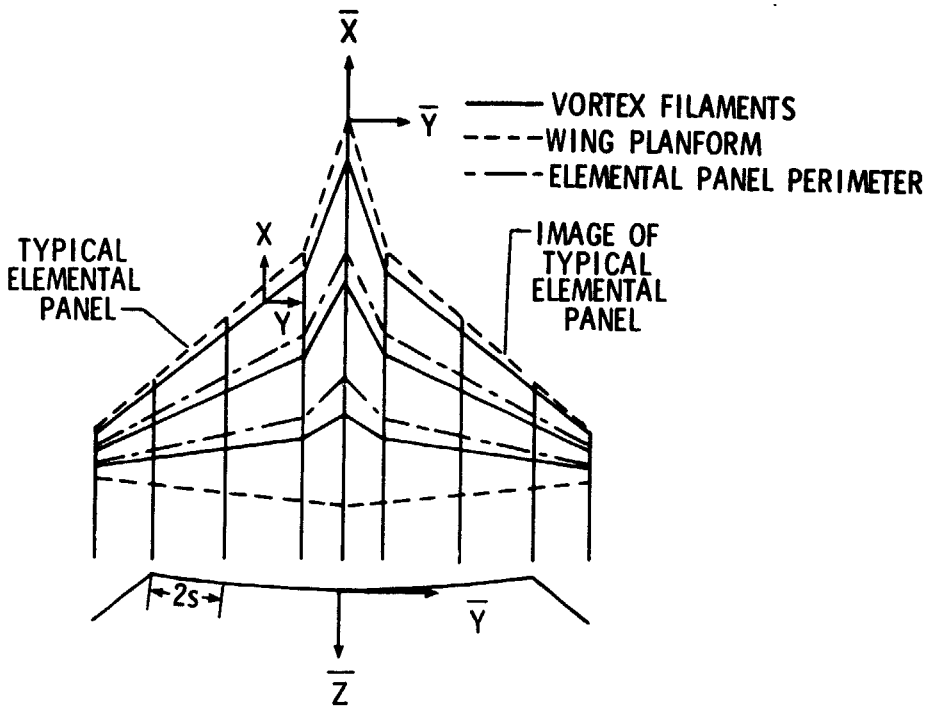

Figure 1.- Axis systems, elemental panels, and horseshoe vortices for typical wing planform.

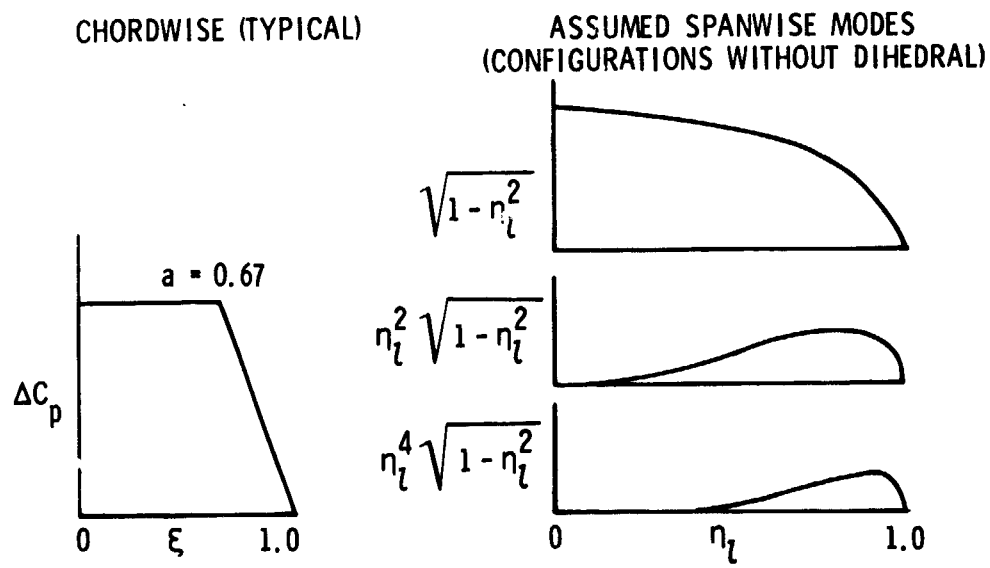

Figure 2.- Planform load distributions.

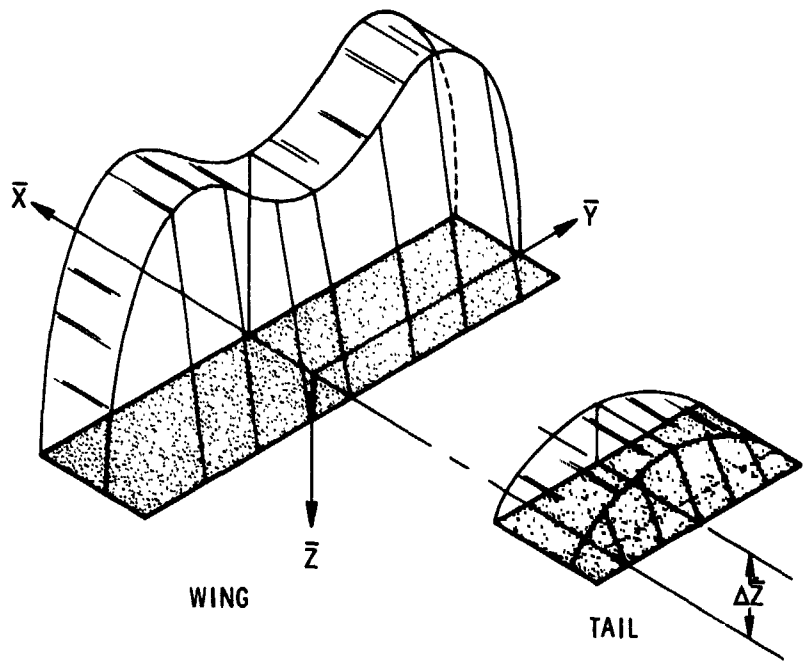

Figure 3.- Idealized loading set on trimmed configuration for minimum drag.

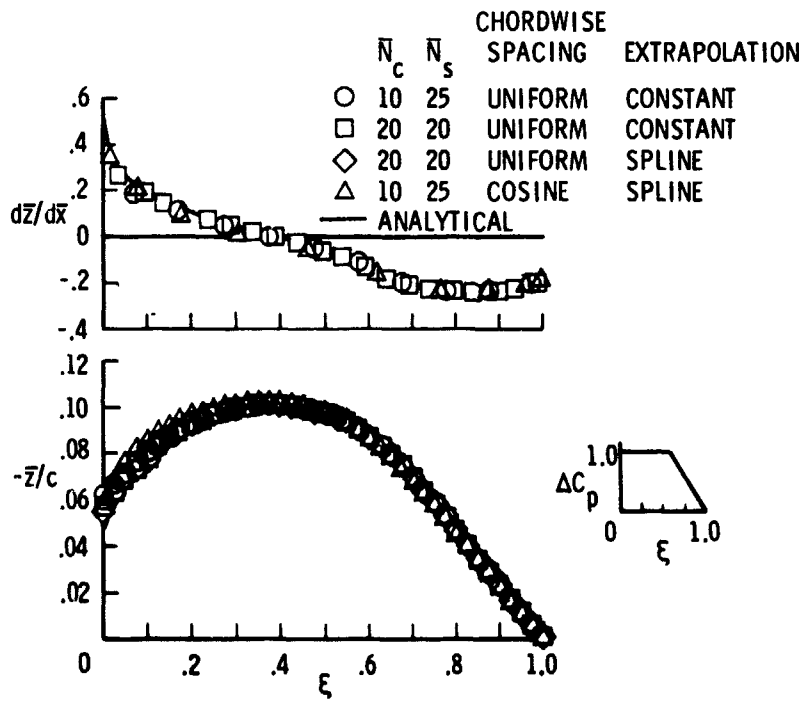

Figure 4.- Two-dimensional local slopes and elevations; a = 0.6.

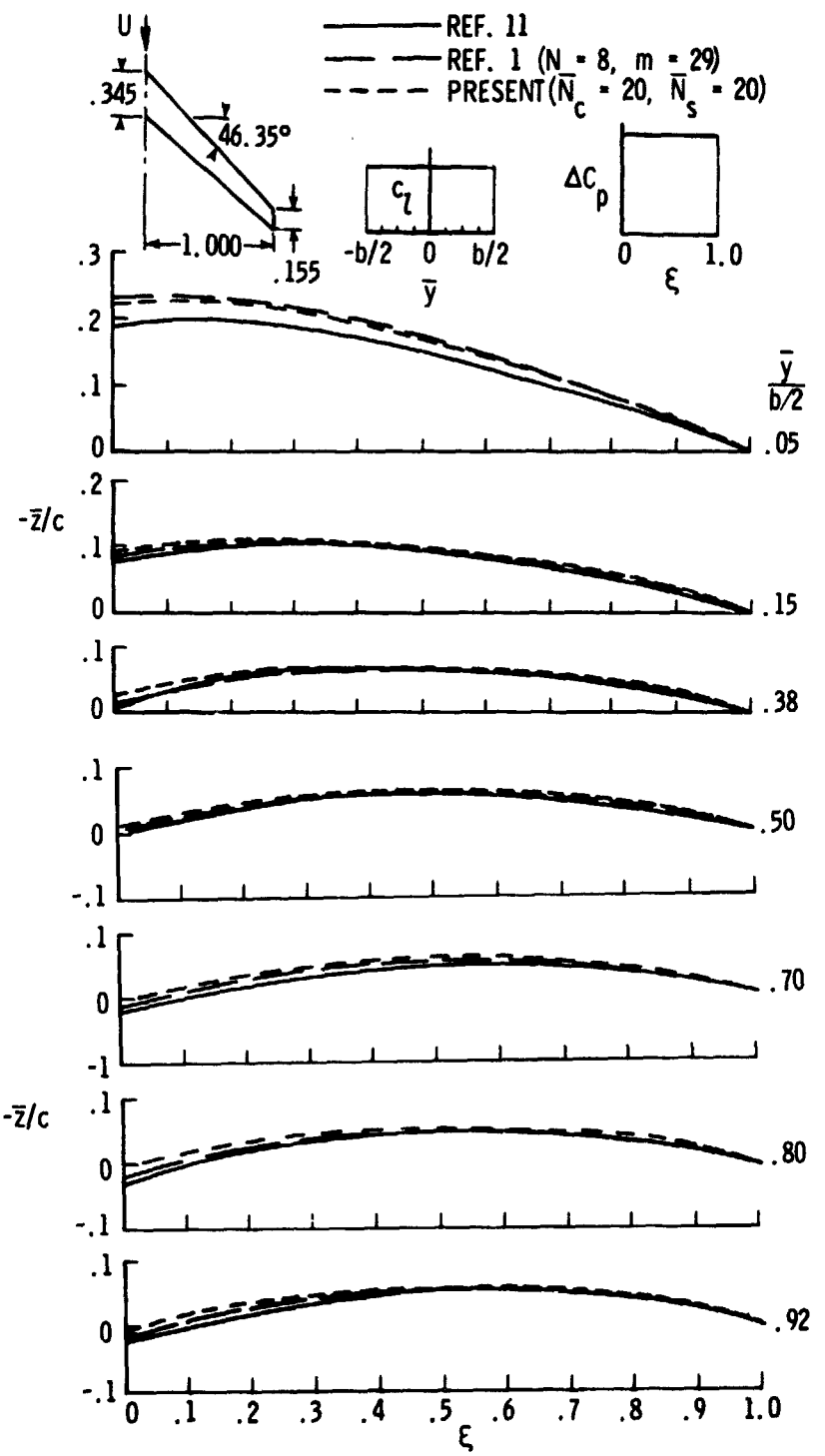

Figure 5.- Local elevation estimates for high-aspect-ratio wing; $C_{L,d}$ = 1.0; M_∞ = 0.90.

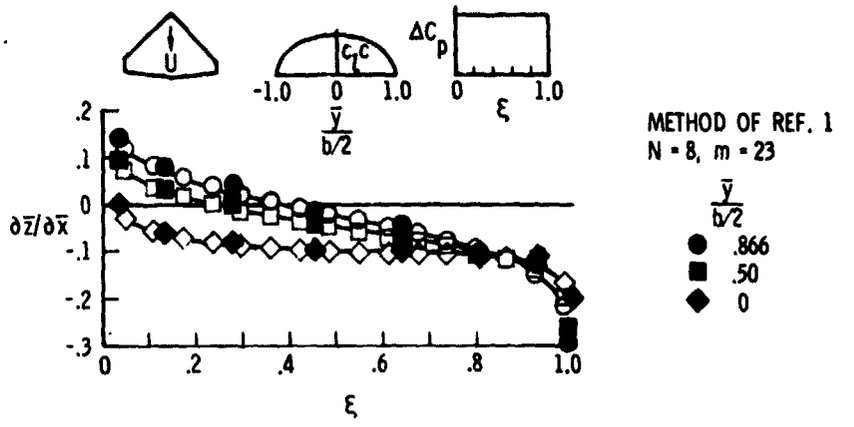

(a) Local slopes.

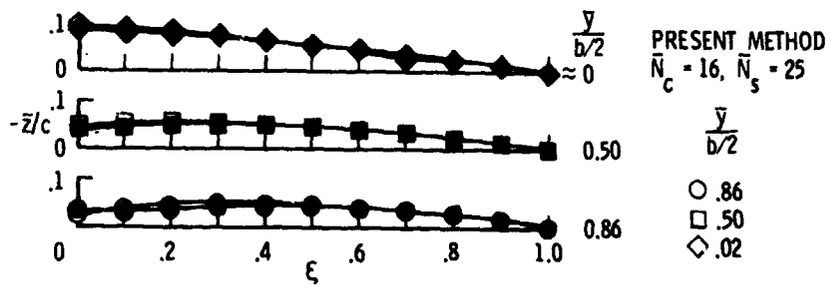

(b) Elevations.

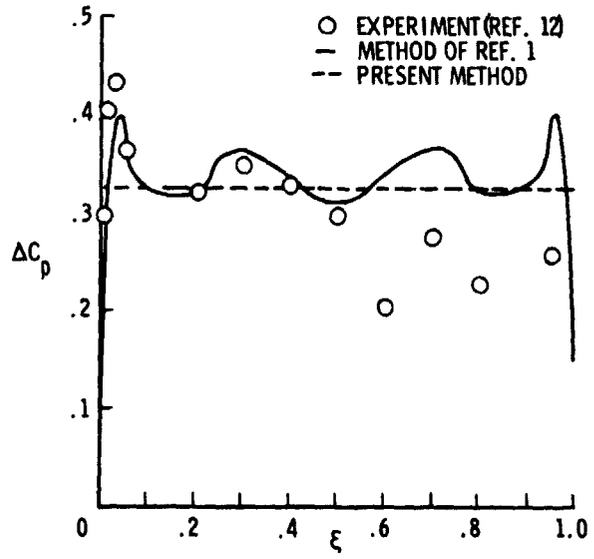

(c) Lifting pressure distributions; $\frac{\bar{y}}{b/2} = 0.259$.

Figure 6.- Local slopes, elevations, and lifting pressure distributions; $C_{L,d} = 0.35$; $M_\infty = 0.40$.

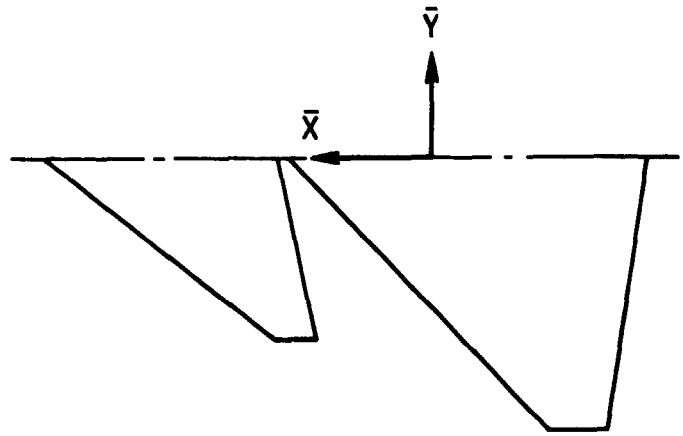

Figure 7.- Typical wing-canard combination.

LINE SYMBOL	a_c	a_w	$C_{L,c}$	$C_{L,w}$	$C_{D,v}$
- - - - - -	0	0	.0338	.1662	.00494
— — —	1	1	.0574	.1426	.00495
———	.6	.8	.0505	.1495	.00495

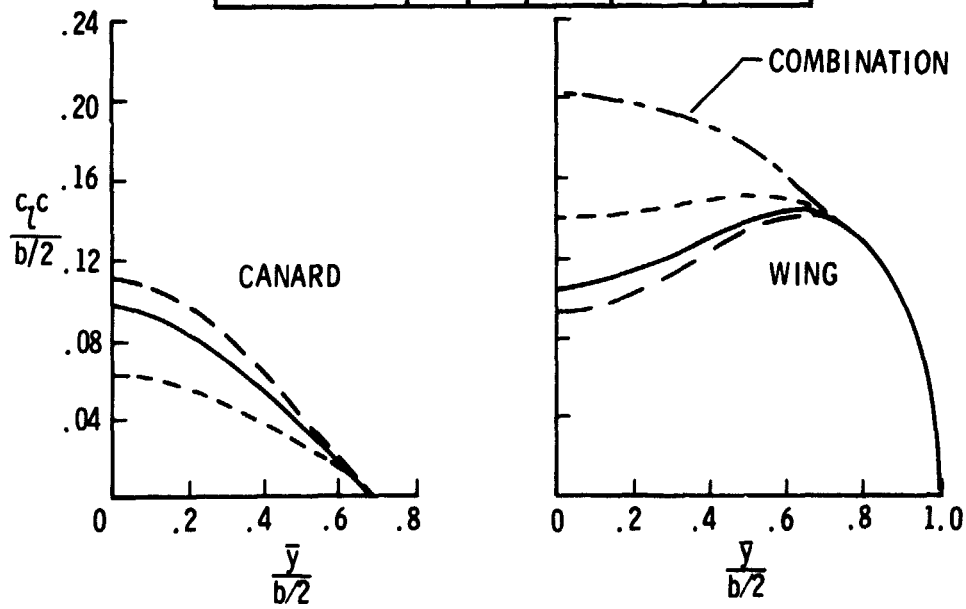

Figure 8.- Effect of chord loading on span loadings for trimmed coplanar wing-canard combination; $M_\infty = 0.30$.

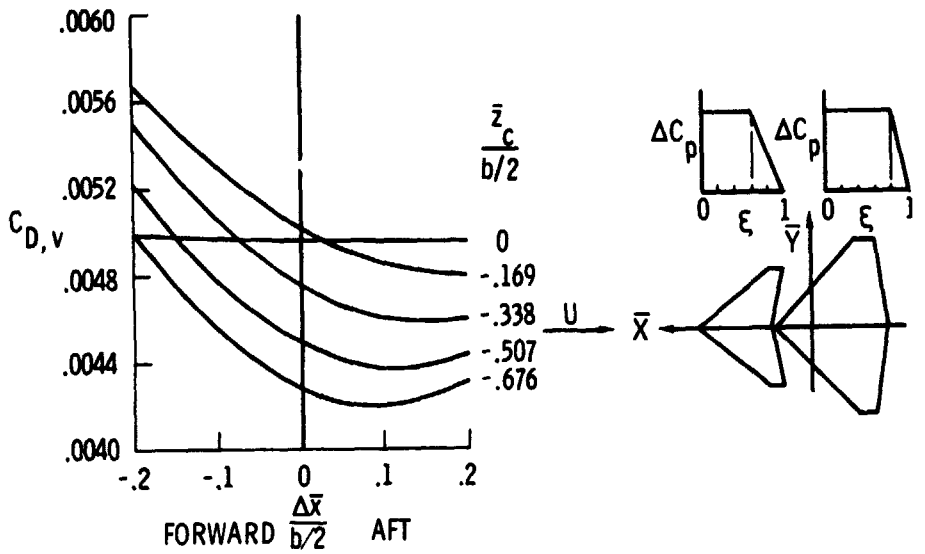

Figure 9.- Vortex drag for range of center-of-gravity positions and vertical separations; $C_{L,d} = 0.2$; $M_\infty = 0.30$.

LINE SYMBOL	$2\bar{z}_c/b$	$C_{L,c}$	$C_{L,w}$	$C_{D,v}$
- - - - - -	-.169	.0498	.1503	.00485
— — —	-.338	.0493	.1507	.00459
— · — · —	-.507	.0491	.1510	.00437
———	-.676	.0489	.1512	.00419

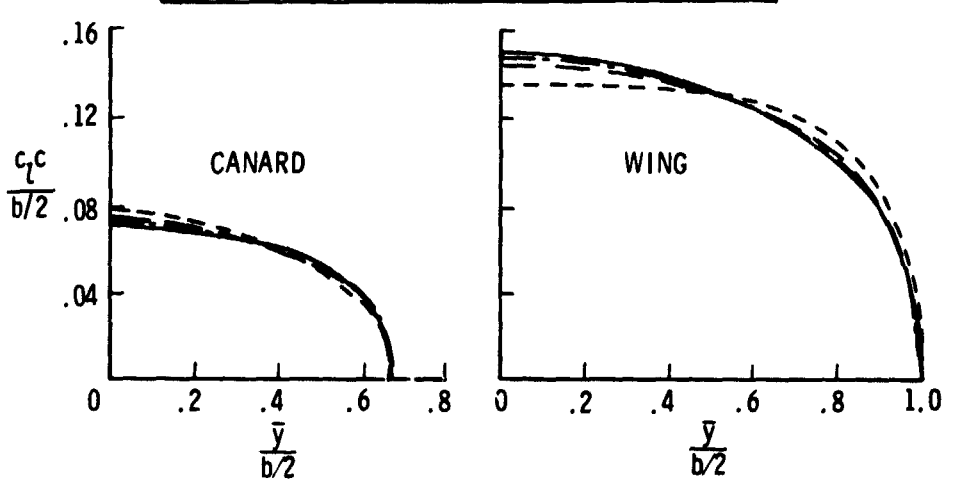

Figure 10.- Effect of vertical displacement of span loadings for trimmed wing-canard combination; $a_c = 0.6$; $a_w = 0.8$; $M_\infty = 0.30$; $\frac{\Delta\bar{x}}{b/2} = 0.10$.

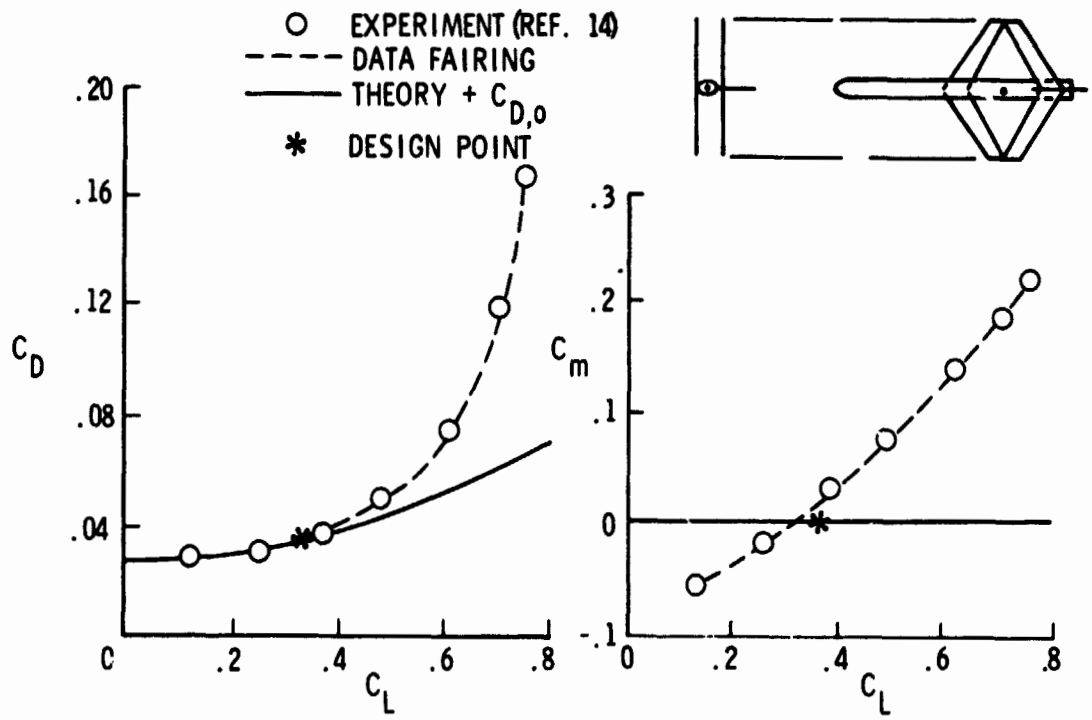

Figure 11.- Longitudinal aerodynamic characteristics of tandem wing; $C_{L,d} = 0.35$; $M_\infty = 0.30$.

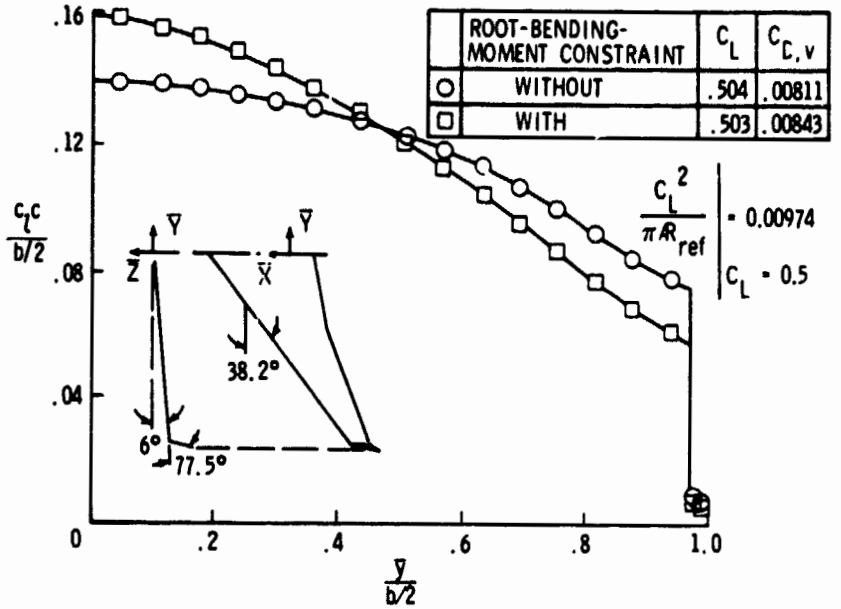

(a) Aerodynamic characteristics.

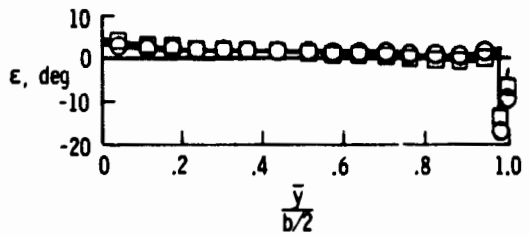

(b) Incidence angle distribution.

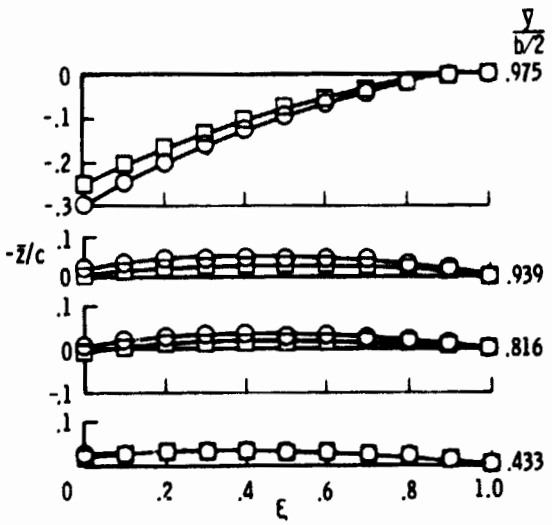

(c) Local elevations.

Figure 12.- Effect of root-bending-moment constraint on aerodynamic characteristics, local elevations, and incidence angle distribution of wing-winglet combination (AR = 6.67); $\bar{N}_c$ = 20; $\bar{N}_s$ = 17; M_∞ = 0.80.